

Visualization of high-speed gas jets and their airblast sprays of cross-injected liquid

K. D. Kihm, T. K. Kim, S. Y. Son

102

Abstract A planar and instantaneous visualization study of high-speed gas jets and their airblast sprays was performed to qualitatively examine the different atomization performances of different gas nozzles. For the visualization of high-speed gas jets (with no liquid injected), Nd:YAG pulsed laser sheets imaged the clustered vapor molecules in the Rayleigh range ($d \ll \lambda$), condensed from the natural humidity during the isentropic gas expansion through a nozzle. This method visualized both underexpanded sonic gas jets from a converging nozzle (SN-Type) and overexpanded supersonic gas jets from a converging-diverging nozzle (CD-Type). When liquid is cross-injected, the same laser sheet images the spray droplets of relatively large sizes ($d \geq \lambda$). The present visualization results show that the SN-Type nozzle develops a wider spray than the CD-Type nozzle, quite probably because the SN-Type nozzle has a wider gas jet (in the absence of liquid) than the CD-Type. Also, the wider spray of the SN-Type nozzle lowers the probability of droplet coalescence and generates finer sprays compared to the CD-Type nozzle. These visualization results qualitatively agree with the previous quantitative finding of the different atomization characteristics of the two types of nozzles (Park et al. 1996).

1

Introduction

The recent work of Park et al. (1996) presents a comparison study of airblast atomization between underexpanded sonic and overexpanded supersonic gas jets. They have measured spray Sauter mean diameters (SMD) for the converging SN-Type nozzle and the converging-diverging CD-Type nozzle using the Malvern technique. The result showed that the SN-Type jet produced persistently smaller sprays, up to 10%, than the CD-Type nozzle, despite the fact that the latter develops a jet with a higher Mach number than the former.

It is conjectured that the injected liquid interactions with the nozzle exit condition, either expansion waves of the SN-Type nozzle (Fig. 1a) or shock waves of the CD-Type nozzle (Fig. 1b), could make noticeable differences in the spray angles, droplet concentrations, probability of droplet coalescence, and droplet

SMDs. In order to qualitatively examine these differences, the present visualization study has been made both for the gas jets, without liquid injected, and the airblast sprays, with liquid cross-injected.

Isentropic expansion of gas, through converging or converging-diverging nozzles, converts its internal thermal energy to kinetic energy for the gas acceleration. The decrease of internal energy significantly lowers the gas temperature and the natural water vapor quickly condenses into molecular clusters of a few nanometers. These molecular clusters are in the Rayleigh range (Long 1977), i.e., $d \ll \lambda$, and can be used as a natural seeding in visualizing high-speed gas jets. The extremely small condensed vapor clusters make excellent tracers with virtually no slip from the high-speed gas flows. A similar method, also known as a vapor-screen (McGregor 1961), has been used to study supersonic shear mixing flows and boundary layers (Desevaux et al. 1994; Pitts and Kashiwagi 1984; Clemens and Mungal 1991; Smith and Smits 1995).

2

Experiment

Figure 2 illustrates the polarization properties of Rayleigh scattering from a spherical particle that is small compared to the wavelength ($d \ll \lambda$). The scattering plane is conformed by the incident light direction (z) and the viewing direction (x or y). Regardless of the polarity characteristics of the incident laser, the Rayleigh scattered light through the 90° viewing angle in x or y , where the maximum image brightness is reached, carries only the polarity component perpendicular to the particular scattering plane. For a plane polarized incident beam, the Rayleigh scattering intensity at the right angle is proportional to the incident beam intensity I_0 and increases inversely with its wave length by an exponent of 4, i.e., $I(\theta = 90^\circ, \perp) = I_0(1/\lambda)^4$.

The experimental system uses a pulsed Nd:YAG laser that generates visible green light ($\lambda = 532$ nm) in the second harmonic mode at 100 mJ per pulse (Kim 1996). The Q-switched mode allows ultra-short pulses of approximately 7 ns up to 10 Hz. When a polarization rotator is aligned for a vertically polarized incident beam (in the y -direction), the horizontal scattering plane x - z must be chosen for viewing since the vertical scattering plane y - z does not contain any Rayleigh scattering intensity at the 90° viewing angle. A combination of concave lens and cylindrical lens converts the laser beam of about 8 mm diameter into a thin sheet of about 0.2 mm thickness near the center. The linear polarizer filter located in front of the image acquiring system (either 35 mm or CCD camera) adjusts the intensity of the Rayleigh scattering

Received: 10 March 1998 / Accepted: 2 November 1998

K. D. Kihm, T. K. Kim, S. Y. Son
Department of Mechanical Engineering, Texas A&M University
College Station, Tx 77843-3123, USA

Correspondence to: K. D. Kihm

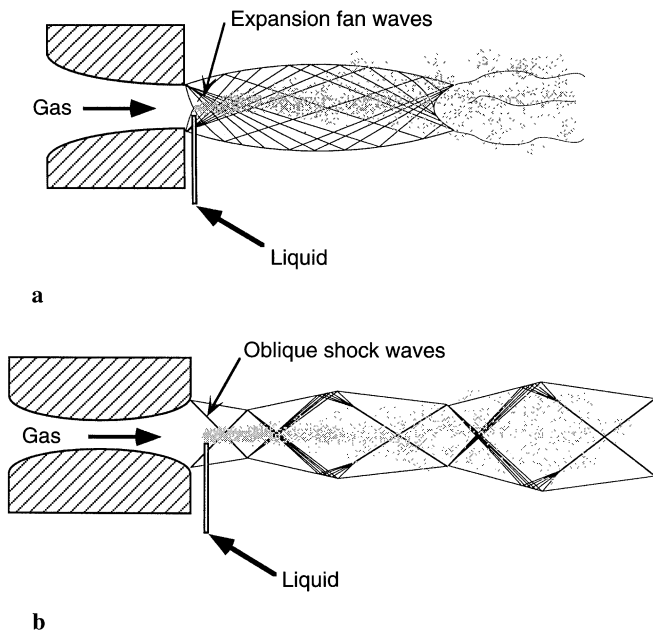


Fig. 1a, b. Schematic of high-speed compressible gas jets. a Underexpanded sonic jet from the SN-type nozzle; b overexpanded supersonic jet from the CD-type nozzle

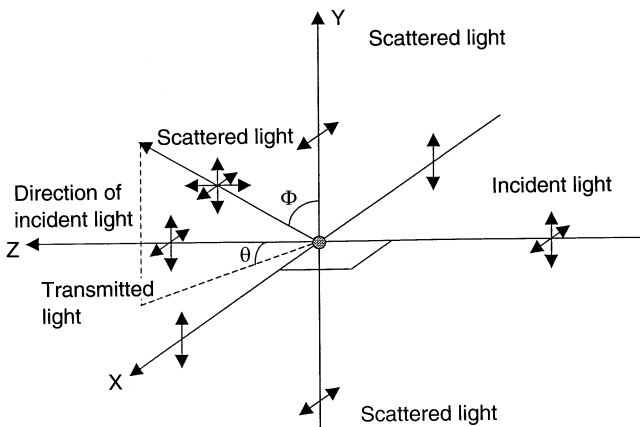


Fig. 2. Polarity changes of Rayleigh scattered light

signal, which yields a maximum with the polarizer filter vertically oriented.

With no liquid injected, the system visualizes the gas jet development by recording images of the naturally occurring mist. When the tested liquid is cross-injected into the high-speed gas jet, the strong airblast atomizes the liquid into fine spray droplets of diameters of relatively larger sizes, i.e., $d \approx \lambda$ or $d \geq \lambda$. Instantaneous images of these droplets visualize the spray development.

3 Results and discussion

The tested SN-Type nozzle has a 2.78 mm exit diameter, and the CD-Type nozzle has a 3.86 mm exit diameter and 3.12 mm throat diameter, with the area ratio of $A/A^* = 1.53$. The gas mass flow rate is calculated from the stagnation pressure and temperature with an isentropic flow assumption (John 1984).

A range of air-to-liquid mass ratio (ALR) was tested for both nozzles.

Figure 3 shows a series of digitally recorded images of air jets exhausted from the SN-Type nozzle at different stagnation pressures. The subsonic jet (Fig. 3a) generates no significant amount of mist since the cold jet is quickly mixed with warm ambience. The starry dots in the background are images of the airborne dust particles. The slightly underexpanded sonic jet (Fig. 3b) develops weak expansion fans and the gas temperature drop will not be sufficient to result in significant condensation. Only a slight amount of mist is shown away from the exit. When the jet is highly underexpanded (Figs. 3c and d), the vapor condensation amount noticeably increases because of the larger temperature drops through the relatively stronger expansion fans.

The subsonic jet of the CD-Type nozzle (Fig. 4a) does not generate any visible condensation. The background images of dust particles have been digitally eliminated this time. At the stagnation pressure range corresponding to Figs. 4b and c, the jet develops the Mach disk (John 1984) near the nozzle exit. The Mach disk occurs when the stagnation pressure is not sufficient to generate full-strength oblique shock waves, and conforms to a normal shock wave of a circular cross-section intervening the initial oblique shock waves (Fig. 1b). The Mach disk, like a normal shock, discontinuously increases both flow pressure and temperature across it and slows down the central portion of the incoming supersonic flow to subsonic flow. This relatively warmer and partially subsonic jet can deteriorate the condensation, and the scattering images of the CD-type nozzle are less distinctive compared with the SN-Type. However, the fully overexpanded jet, with no Mach disk, generates sufficient amount of mist to clearly visualize the jet development (Fig. 4d).

Despite the fact that the exit area of the SN-Type nozzle is approximately one half of the CD-Type nozzle, the jet diameter and divergence of the former (Fig. 3d) are not any smaller than those of the latter (Fig. 4d). As shown schematically in Fig. 1, the overexpanded flow from the CD-Type nozzle contracts toward the centerline immediately after it emerges, whereas the underexpanded jet from the SN-Type nozzle radially expands as it emerges. The more definite contact surface is formed by the stronger shock cell pattern of the CD-Type jet, while the relatively weaker contact surface is formed by expansion fans for the case of the SN-Type nozzle. The stronger contact surface tends to restrict the jet divergence. As a result of this, the CD-Type nozzle develops a narrower jet than the SN-Type nozzle.

Figure 5 shows spray images of the SN-Type nozzle for a constant water flow rate of $\dot{m}_L = 0.9$ g/s at different airflow rates. During the transition from subsonic (Fig. 5a), nearly isentropic sonic (Fig. 5b) to underexpanded sonic (Fig. 5c), the spray angle remains unchanged and the spray development maintains similarity. The less bright images are recorded with increased air-to-liquid ratio (ALR) since the spray droplet concentration is lowered by dispersion.

Figure 6 shows spray images under airblast by the CD-Type nozzle. The liquid injection rate is increased to $\dot{m}_L = 1.13$ g/s in proportion to the 25% increase in the throat area compared with the SN-type nozzle. The spray angle noticeably decreases during the transition from subsonic (Fig. 6a) to supersonic

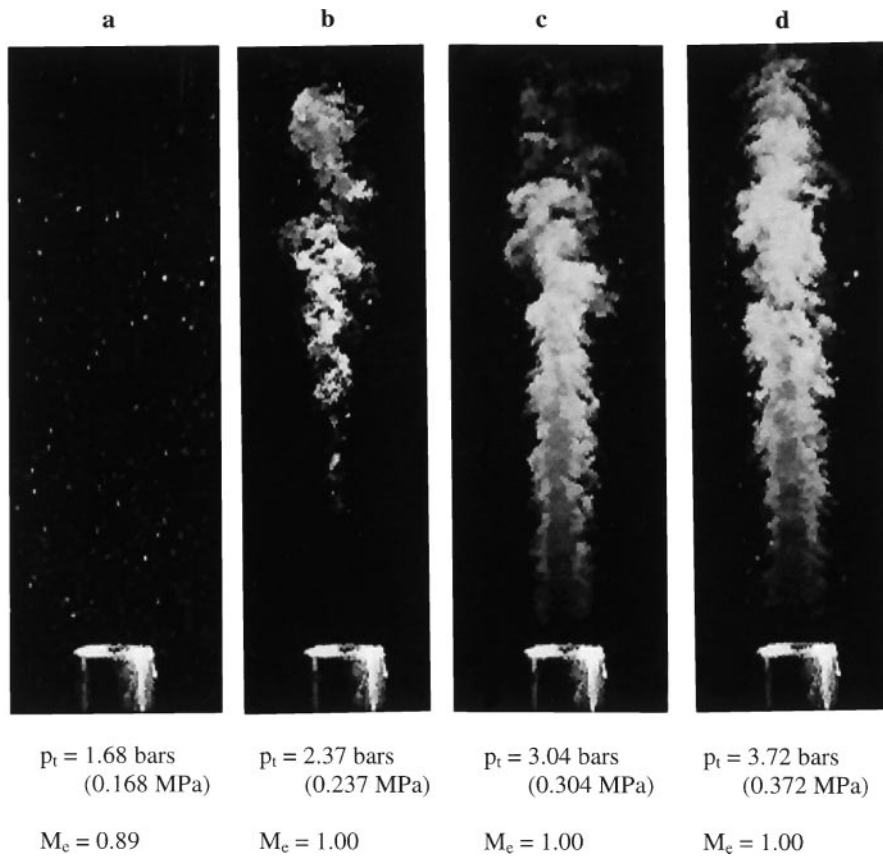


Fig. 3a–d. Rayleigh scattering images of air jets exhausting from the SN-type nozzle

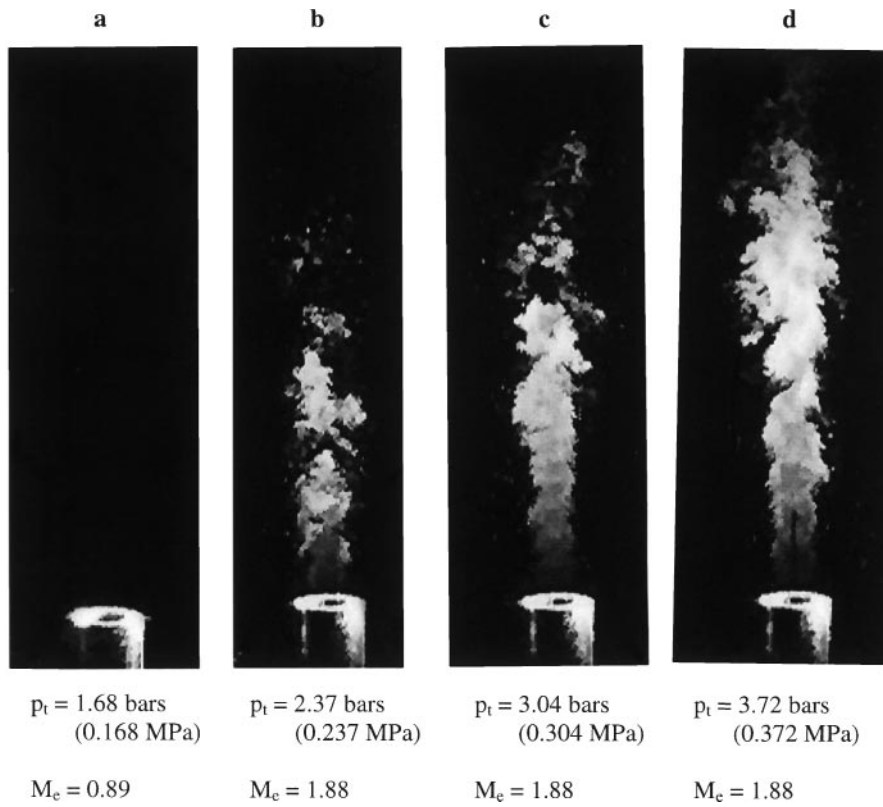


Fig. 4a–d. Rayleigh scattering images of air jets exhausting from the CD-type nozzle

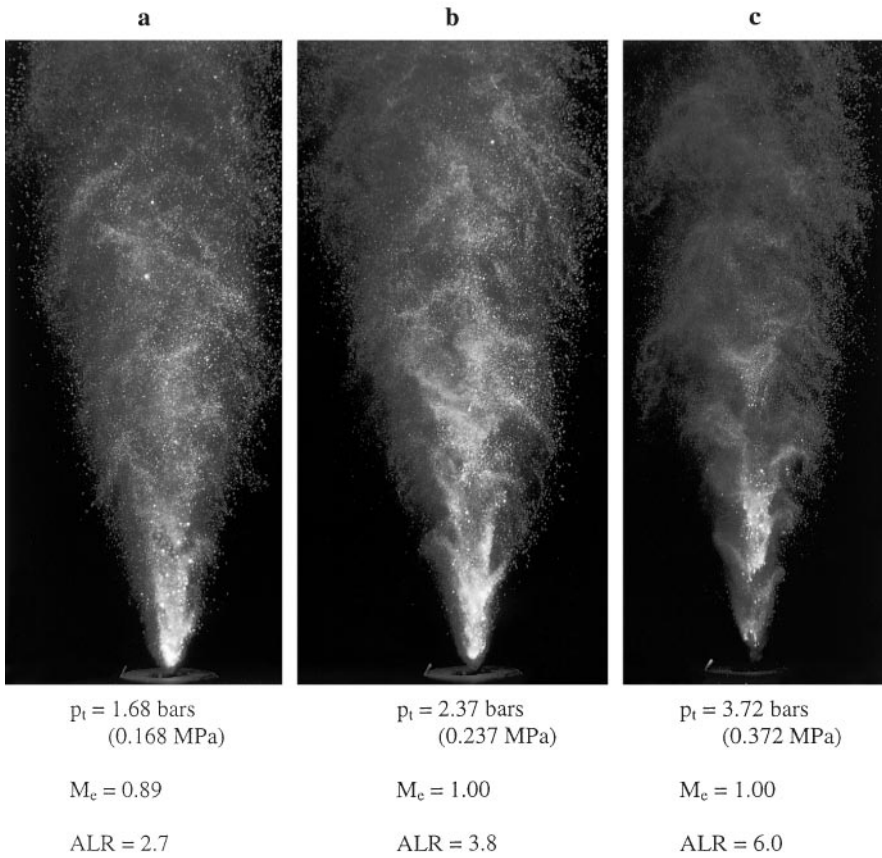


Fig. 5a–c. Spray images of the SN-type nozzle for constant liquid flow rate, $\dot{m}_L = 0.9$ g/s

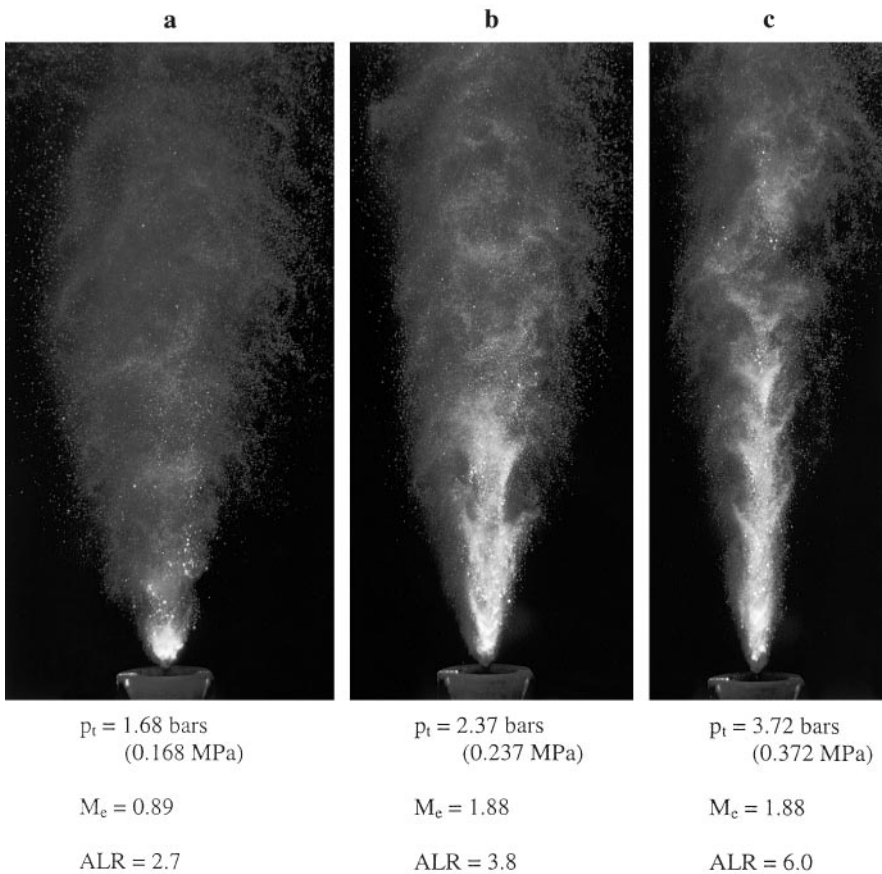


Fig. 6a–c. Spray images of the CD-type nozzle for constant liquid flow rate; $\dot{m}_L = 1.13$ g/s

(Fig. 6b and c) with increasing ALR. The spray density increase by the reduced spray cross-section overrides the spray dispersion occurring with increasing ALR. Thus, the overall droplet concentration increases with increasing ALR and the spray image is brighter because of the intenser scattering. The increased droplet concentration of the CD-Type sprays, because of its narrower spray development, also increases the probability of droplet coalescence.

4

Concluding remarks

The spray angle of the CD-Type nozzle gradually decreases with increasing ALR since the contact surface strength increases. The overexpanded supersonic air jet, from the CD-Type nozzle, contracts inward and tends to more strongly restrict the liquid spray within its contact surfaces, and consequently, develops a narrower spray. On the other hand, the SN-type nozzle develops weaker contact surface with radially outward expansion, and its strength does not significantly increase with increasing ALR. Thus, the SN-Type nozzle develops similar spray angles regardless of ALR. The narrower spray of the CD-Type nozzle increases the chance of droplet coalescence and contributes to increasing the spray drop SMDs compared to the relatively wider spray of the SN-Type nozzle. The present qualitative visualization results support for the previous finding of Park et al. (1996): the slightly better atomization performance measured for the SN-Type nozzle, in comparison with the CD-Type nozzle.

References

- Clemens NT; Mungal MG** (1991) A planar Mie scattering technique for visualizing supersonic mixing flows. *Exp Fluids* 11: 175–185
- Desevaux P; Prenel JP; Hostache G** (1994) An optical analysis of an induced flow ejector using light polarization properties. *Exp Fluids* 16: 165–170
- John JEA** (1984) *Gas dynamics*. 2nd ed. Prentice-Hall, Englewood Cliffs
- Kim TK** (1996) Investigation of sonic/subsonic air-blast atomization using Rayleigh- and Mie-scattering visualization technique. M.S. Thesis. Department of Mechanical Engineering, Texas A&M University, College Station
- Long DA** (1977) *Raman spectroscopy*. McGraw-Hill, New York
- McGregor I** (1961) The vapor-screen method of flow visualization. *J Fluid Mech* 11: 481–511
- Park BK; Lee JS; Kihm KD** (1996) Comparative study of twin-fluid atomization using sonic or supersonic gas jets. *Atomization and Sprays* 6: 285–304
- Pitts WM; Kashiwagi T** (1984) The application of laser-induced Rayleigh light scattering to the study of turbulent mixing. *J Fluid Mech* 141: 391–429
- Smith MW; Smits AJ** (1995) Visualization of the structure of supersonic turbulent boundary layers. *Exp Fluids* 18: 288–302